Quantum Intermixing For Monolithic Integration of Different Optoelectronic Devices

P.L. Gareso
Department of Physics, Faculty of Mathematics and Natural Sciences, Hasanuddin University
Makassar 90245, Indonesia
pgareso@fmipa.unhas.ac.id

1. Introduction

The monolithic integration of photonic/optoelectronic devices into a single chip is of great advantages integrated circuits have over discreate components. Two methods are commonly used to achieve this: selective area epitaxy and etch-and-regrowth on a patterned substrate. However, both of these techniques are complicated and costly. An alternative technique that can be applied to the monolithic integration is a post growth intermixing. The post growth intermixing technique is the simplest technique compared to other methods and relies on the atomic intermixing between the quantum and barriers region. This results in the grading of the initially abrupt interfaces hence a blue shift of the quantum region emission. Intermixing in the active region can be achieved by several techniques including ion implantation [1-3], impurity induced disordering [4], and impurity free vacancy disordering (IFVD) [5,6]. Intermixing by ion irradiation followed by annealing has been shown to be very effective to modify the band gap since it enable precise control of the defects that are introduced into the sample, simply by varrying the irradiation conditions. Moreover, a very high degree of reproducibility can be achieved. Meanwhile, IFVD has shown to be very effective for device application since it is simple and the amount of residual defects that are created by the intermixing process is much lower than by ion implantation and impurity difusion.

The purpose of this paper is to study two methods that are used to modify the band gap energy namely: ion implanation and IFVD. Two different different material system, InGaAs/InP quantum structures and InGaAs/AlGaAs quantum laser structures were used to study the intermixing mechanism.

2. Experimental Details

2.1. IFVD Technique

The laser structure used was grown on a (100) n^+ GaAs substrate using low pressure metalorganic chemical vapor deposition (LP-MOCVD). We used a thin p-$Al_{0.6}Ga_{0.4}As$ cladding layer structure which uses the asymmetric design of the optical distribution that most of it lies in the n-type layers and only small part of the distribution is found near the top surface. In addition, the structure is well suited to the intermixing in the GaAs based system, where the diffusion length of Ga Vacancies is of the order of 0.1 µm. The thin p-cladding layers have a nominal thickness of 0.3 µm and $5x10^{17}$ cm^{-3} doping level. The top p^{++} GaAs contact layer was highly doped ($>5x10^{19}$ cm^{-3}). Both the p-cladding layer and the GaAs contact layer were doped with carbon using CCl_4. The active region consists of two $In_{0.20}Ga_{0.80}As$ undoped QWs which were separated by $Al_{0.20}Ga_{0.80}As$ barrier layers, while the bottom n-type cladding layers were doped with Si. Detailes of the structures are summarized in Table.1. Silicone dioxide with of thickness of 200 nm was deposited by plasma-enhaced chemical vapor deposition (PECVD) using a N_2O/SiH_4 mixture at room tempearture. On each half of the samples, SiO_2 layers were removed by 10% HF after deposition to provide a reference region. TiO_2 layers with a nominal thickness of 200 nm were deposited by electron beam evaporation. In order to provide a reference, a half of each sample was covered with a mask prior to the TiO_2 depostion. All the samples were annealed under Ar flow in a rapid thermal annealer in the temperature range of 875-925^oC for 60 s. During annealing, the samples were sandwiched between two GaAs substrate to minimize arsenic loss from the samples.

Tabel. 1. Details of the asymmetric InGaAs/AlGaAs QW laser structures used in this work.

Layer Type	Al composition index	Thickness	Doping
p^{++}GaAs	0.00	0.10 μm	C >1x10^{19} cm^{-3}
p $Al_xGa_{1-x}As$	0.60	0.30 μm	C~1x10^{18} cm^{-3}
Grading $Al_xGa_{1-x}As$	0.60 → 0.20	0.16 μm	Undoped
GaAs	0.00	1.8 nm	Undoped
$In_{0.20}Ga_{0.80}As$		6 nm	Undoped
GaAs	0.00	1.8 nm	Undoped
$Al_xGa_{1-x}As$	0.20	6 nm	Undoped
GaAs	0.00	1.8 nm	Undoped
$In_{0.20}Ga_{0.80}As$		6 nm	Undoped
GaAs	0.00	1.8 nm	Undoped
Grading $Al_xGa_{1-x}As$	0.20 → 0.60	0.16 μm	Undoped
$Al_xGa_{1-x}As$	0.60	0.10 μm	Si: 10^{17} cm^{-3}
Grading $Al_xGa_{1-x}As$	0.60 → 0.30	0.02 μm	Si: 10^{17} cm^{-3}
$Al_xGa_{1-x}As$	0.30	0.22 μm	Si: 10^{17} cm^{-3}
Grading $Al_xGa_{1-x}As$	0.30 → 0.45	0.01 μm	Si: 10^{17} cm^{-3}
$Al_xGa_{1-x}As$	0.45	0.07 μm	Si: 5x10^{17} cm^{-3}
$Al_xGa_{1-x}As$	0.45	2.00 μm	Si: 10^{18} cm^{-3}
n^+substrate			

2.2. Ion Implantation

Three samples of InGaAs/InP QWs were grown on semi-insulating (100) InP substrate by MOCVD at 650^{o}C. The indium composition was nominally 0.38, 0.53 and 0.68 corresponding to tensile-strained (TS), lattice-matched (LM) and compressively-strained (CS) QWs, respectively. Each of the samples was comprised of 600 nm InP, 5 nm thick $In_xGa_{1-x}As$ QW and 400 nm InP. Proton irradiation was carried out using 500 kV ions with doses ranging from 5x10^{14} H cm^{-2} to 1x10^{16} H cm^{-2}. Based on TRIM simulation at 50 keV, the peak of the damage profile lies in the quantum well region. The irradiation temperature was varried from room temperature to 300^{o}C. During implantation, half of each of the samples was masked to provide a reference. Subsequent thermal annealing was performed under Ar flow in a rapid thermal annealer (RTA) at 750oC for 60 s. This temperature was choosen after our study of thermal interdiffusion which showed that at this temperature, the diffusion caused by thermal component could be kept low. Thus, by annealing the implanted samples at this temperature, any measured peak energy shift could be assigned solely to the effect caused implantation.

Low temperature PL (77 K) was performed on both IFVD and ion implantation samples to characterize the energy shift in the quantum well region using a diode-pumped solid-state frequency-doubled green laser at 532 nm for excitation and a cooled InGaAs photodetector at the output slit of a 0.5 m monochromator.

3. Results and Discussion

3.1. SiO_2 and TiO_2 dielectric layers

Figure.1 shows the low temperature (77K) photoluminescence spectra of as-grown sample and also the samples annealed with SiO_2. For the as-grown sample, the luminescence peak was observed at 903 nm due to recombination in the InGaAs quantum well active region. For SiO_2 cap layers, the PL linewidth and the PL intensity did not change significantly after annealing at 875^{o}C, which indicates that the good quality of the quantum well was maintained although there was a slight blueshift. On the other hand, the PL intensity decreased significantly after annealing at 925^{o}C in comparison to the as-grown samples, and a progressively more blueshift was observed with increasing annealing temperature for the SiO_2 capped samples.

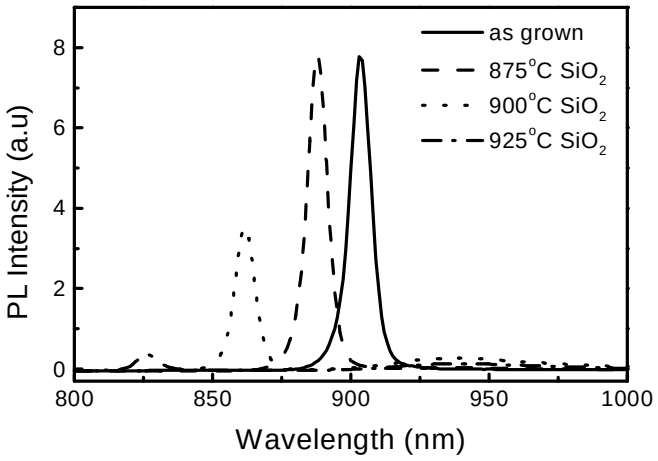

Figure.1: Low temperature (77K) photoluminescence (PL) spectra of as-grown sample and after annealing in the temperature range of 875 – 925°C for 60 sec with SiO_2 cap layer.

It also shows in Figure. 1, at 900°C-925°C, a large energy shift was observed in the samples capped with SiO_2 layers. It is well known that SiO_2 acts as a ``sink'' for Ga atoms during annealing. Ga atoms outdiffuse from GaAs and generate vacancies. During the RTA, these vacancies diffuse deep into the quantum well and promote the intermixing process. In addition to this, the strain at the GaAs/dielectric interface might influence the intermixing [5]. Since the thermal expansion coefficient of SiO_2 (~0.52×10^{-6} $^oC^{-1}$) is smaller than GaAs (~6.86×10^{-6} $^oC^{-1}$) (see table 2), during RTA, the GaAs surface is under compressive stress which is favourable for the diffusion of these vacancies. Thereby, the diffusion of the V_{Ga} generated below the GaAs/dielectric interface is further enhanced across the QW to create more intermixing.

Figure 2 shows the low temperature photoluminescence spectra of the as-grown samples, annealed samples without cap layers at 925°C for 60 and TiO_2 capped samples annealed at various temperatures from 875°C to 925°C for 60 sec. It can be seen from this figure that a large energy shift (50 meV) was observed in the samples without cap layer compared with the as-grown samples. Also, a relatively broad peak at 942 nm was observed. This peak is attributed to the point defects which are thermally generated during annealing. In the case of TiO_2 cap layers, annealing the samples up to 925°C resulted in very little shift compared with the as-grown samples. The results indicated that thermal intermixing was greatly suppressed by the presence of a TiO_2 layers on the top of the GaAs contact layer. It is worth noting that the broad peak at 942 nm was not observed in the TiO_2 case. This suggests that the TiO_2 effectively suppressed the exchange of atoms during annealing and prevented the generation of point defects. The reason for suppression of interdiffusion by TiO_2 has previously reported [5] and is related to the difference in the thermal expansion coefficient between the semiconductor and the TiO_2 layer. Tensile stress imposed by the TiO_2 on the semiconductor suppresses the diffusion of point defects (group III vacancies that cause interdiffusion. The layer of TiO_2 also suppresses the additional electrical activation of the carbon atoms in comparison to a sample without a capping layer.

Table.2. Thermal expansion coefficient of GaAs, SiO_2 and TiO_2

Material	Thermal Expansion coefficient (10^{-6} $^oC^{-1}$)
GaAs	6.86
SiO_2	0.52
TiO_2	8.19

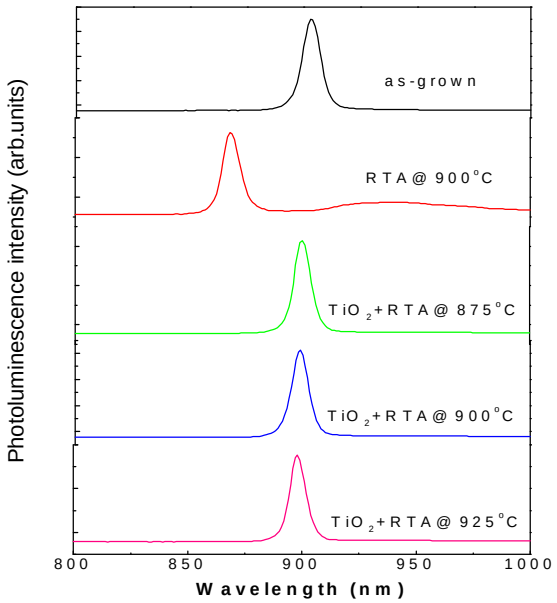

Figure.2. Low temperature (77K) photoluminescence spectra of as-grown sample and after annealing in the temperature range of 875 – 925°C for 60 sec with TiO_2 cap layer PL spectrum from the samples

3.2. Device fabrication

Standard device processing techniques were applied to fabricate the 4 μm wide stripe laser devices. The p-ohmic contact was obtained by evaporating Au on the top p++GaAs contact layer. The contact was unannealed in order to prevent optical attenuation due to radiation scattering at the Au/p++/GaAs interface. The laser diodes were tested using an integrating sphere and a InGaAs photodiode.

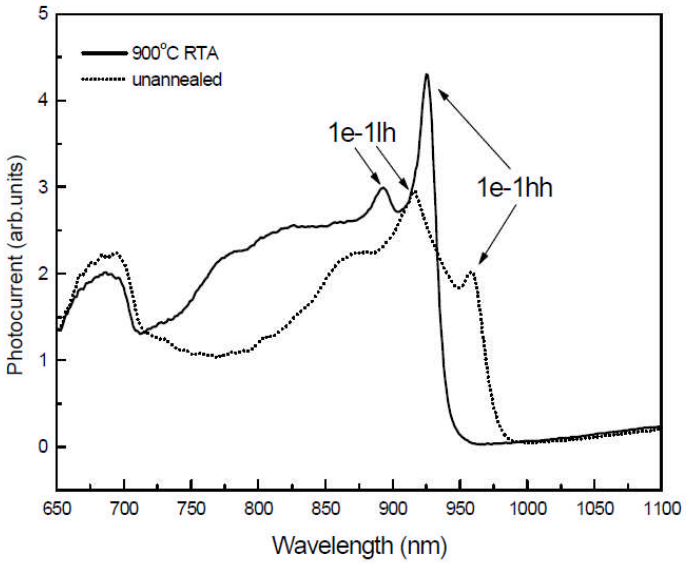

Figure3. Room temperature photocurrent in C-doped InGaAs/AlGaAs laser structures. The solid line represents the photocurrent after annealing at 900°C for 60s and the dotted line represents the photocurrent before annealing.

The relative photocurrent response of C-doped InGaAs/AlGaAs laser structures at zero bias is displayed in figure.3 at room temperature. When the photon energy (hν) is larger than the band gap of the sample, light is absorbed and photocarriers are generated. After annealing, the quantum well peak emerges at 925 nm, which is blue shifted around 33 nm from the asgrown sample. This result agrees well with what we observe in the PL measurement at room temperature. In addition, the relative intensity of the 1e-1hh transition after annealing is much higher than before annealing and the peak becomes narrower. It suggests an improved quality of the quantum well active region after annealing. In addition, the intermixing must have affected the In and Al content in the barriers between the two quantum wells, leading to an increase of the oscillator. strength of the 1e-1hh transition and to a shallower confining potential for electrons and holes. These effects are beneficial for laser operation since the 1e-1hh transition is the one that provides the gain for lasing and a shallower potential allows a more uniform carrier concentration in the two quantum wells.

The laser structures were processed into 4 μm wide stripe, ridge waveguide devices using standard procedures. Devices were then characterized by plotting the external differential efficiency η and threshold current as a function of cavity length. The internal efficiency and the optical loss α are then extracted from the intercept and slope of the graph. Figure 4a shows a plot of inverse external quantum efficiency against cavity length before and after annealing. The internal absorption coefficient αi after annealing is around 2.6 cm-1 and 2.8 cm-1 before annealing. The device series resistances before and after annealing are comparable. Figure 4b presents a plot of the threshold current against cavity length. It was clearly observed that the threshold current decreased by approximately four times after annealing, most likely due to the activation of the carbon dopant. These results show that not only there is no significant degradation of device lasing parameters, but a significant improvement in the threshold current is seen after annealing.

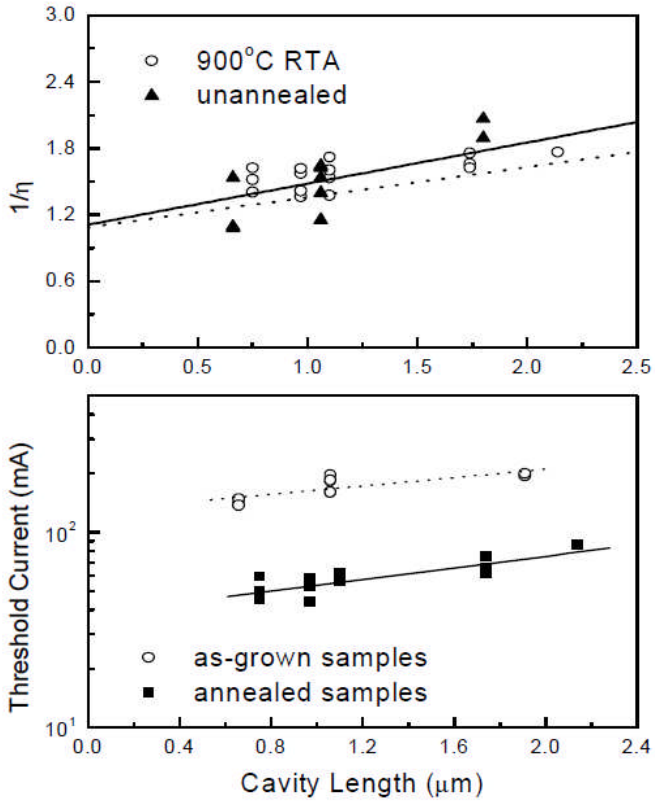

Figure.4. C-doped InGaAs/AlGaAs laser diodes. a) the inverse of the differential efficiency against cavity length before and after annealing, b) a plot of the threshold current with different cavity length of devices.

3.3. Ion Implantation
3.3.1. Photoluminescence

Figure.5 shows the PL spectra at 77 K of the three as-grown samples. For LM and CS QWs, each of peak corresponds to the exitonic recombination between electron and heavy holes from the n=1 subband levels (C-HH), while for TS QWs, the peak is related to the exitonic recombination of electron and light holes from n=1 subband levels (C-LH) of InGaAs QWs. As can be seen from figure 5, the peak position of TS QW was at 1280 nm. This peak position was shifted to a higher wavelength of 1393 nm for LM structures and 1555 nm for CS structures, respectively, as the indium composition in InGaAs Qws was increased. These changes in the peak position of the quantum wells are due to changes in indium composition and strain. Also, it is worth noting that the high PL peak intensity, and narrow, small and symmetrical linewidth of the peak emission of the samples were relatively similar for LM, TS and CS indicating the smoothness of interfaces and homogeneous thickness of each of the InGaAs QW after growth.

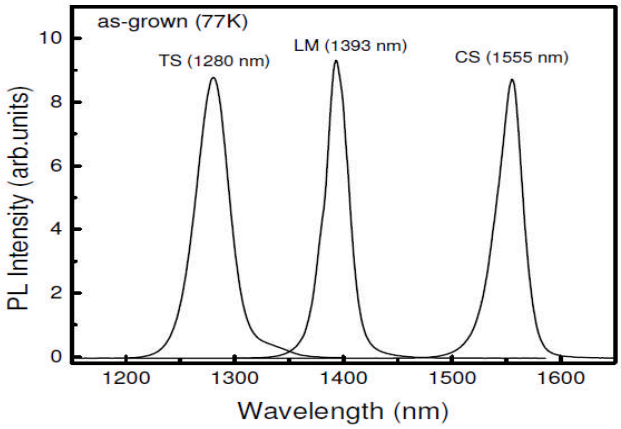

Figure 5. Low temperature PL spectra of as-grown tensile-strained (TS), lattice-matched (LM) and compressively-strained (CS) $In_xGa_{1-x}As/InP$ QWs.

Figure.6 displays the 77K PL spectra for implanted TS, LM and CS QW samples annealed at 750°C for 60 s for doses ranging from $5x10^{14}$ H cm^{-2} to $1x10^{16}$ H cm^{-2}. It can be clearly seen from this figure that after implantation, blue shift was observed for all implanted and annealed samples in comparison to the reference samples (unimplanted and annealed). However, the magnitude of the energy shift became saturated at high implantation doses, followed by a reduction of the PL intensity and the broadening of the PL linewidth. It is worth mentioning that prior to annealing, PL emission was not observed due to defects that formed after irradiation which act as non-radiative recombination centres. After annealing the PL emission was recovered, but the PL intensities were still lower than unirradiated samples indicating that defects were still present and not sufficiently removed after annealing at this temperature. It also clearly seen that the energy shift initially increased as the dose was increased and it reached a maximum at $5x10^{15}$ H cm^{-2}. As the dose was further increased to $1x10^{16}$ H cm^{-2}, a saturation in the energy shift was observed. These results are in contrast to the previous studies of InGaAs/AlGaAs and AlGaAs/GaAs QWs using proton irradiation in which energy shift was not saturated even at the highest doses ($5x10^{16}$ H cm^{-2}). This may due to differences in the types of defects formed in various material systems. In addition to this, it is well known that in AlGaAs/GaAs and InGaAs/AlGaAs system, the well-barrier interdiffusion during the annealing occurs only on the group III sublattice.

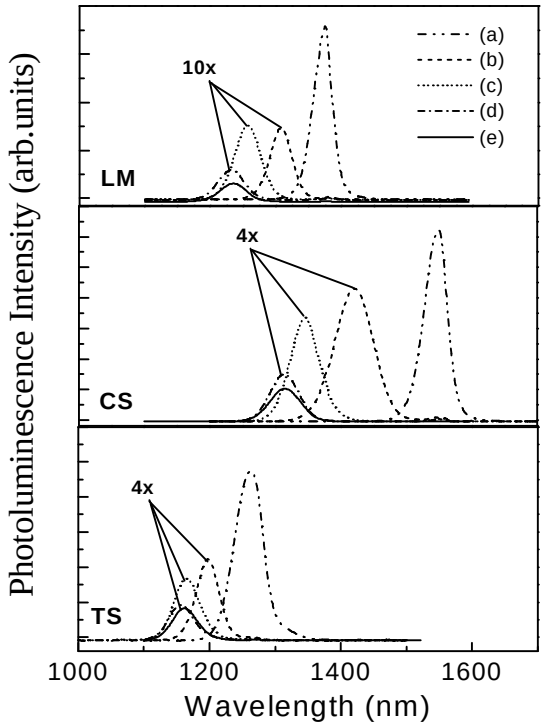

Figure.6: The PL spectra of lattice-matched (LM), compressively-strained (CS), and tensile-strained (TS) QW samples, after implantation and annealing at 750°C for 60 sec. (a) unimplanted and annealed sample for reference, (b)$5x10^{14}$ H/cm^2, (c)$1x10^{15}$ H/cm^2, (d)$5x10^{15}$ H/cm^2, (e)$1x10^{16}$ H/cm^2.

4. Conclusion

We have studied the atomic intermixing of quantum well samples using IFVD and ion implantation method. For IFVD technique (InGaAs/AlGaAs), it was clearly seen that a large energy shit occurring if the samples were covered with SiO2, while the suppression taking place using the TiO_2 dielectric layers. The use of proton implantation with different doses in InGaAs/InP QWs samples implies to modify the bandgap energy. These results show that the use of two methods is very attractive option for optoelectronic integration.

References

[1]. H. H. Tan, J. S. Williams, C. Jagadish, P. T. Burke, and M. Gal, "Large energy shifts in GaAs-AlGaAs quantum wells by proton irradiation-induced intermixing," *Appl .Phys. Lett.* **68**, pp. 2401-2403, 1996.

[2]. H. H. Tan and C. Jagadish, "Wavelength shifting in GaAs quantum well lasers by proton irradiation," *Appl .Phys.Lett.* **71**, pp. 2680-2682, 1997

[3]. P. L. Gareso, M. Muda, L. Fu, H. H. Tan, C. Jagadish, L.V. dao, X. Wen, and P. Hannaford, "Proton irradiation-induced intermixing in $In_xGa_{1-x}As$/InP quantum wells – the effect of In composition" .", Semicond.Sci. Technol, 21, pp 1441-1446, 2006.

[4]. D. G. Deppe and N. Holonyak, Jr., "Atom diffusion and impurity-induced layer disordering in quantum well III-V semiconductor heterostructures," *J. Appl .Phys.* **64**, pp. R93-R113, 1988

[5]. L. Fu, P. Lever, H. H. Tan, C. Jagadish, P. Reece, and M. Gal, "Suppression of interdiffusion in InGaAs/GaAs quantum dots using dielectric layer of titanium dioxide," *Appl .Phys. Lett.* **82**, pp. 2613-2615, 2003.

[6]. P.L. Gareso, M. Buda, L. Fu, H. H. Tan, and C. Jagadish, " Suppresion of termal atomic interdiffusion in C-doped InGaAs/AlGaAs quantum well laser structures using TiO_2 dielectric layers", Appl. Phys. Lett, 85, pp 5583-5585.